





Hydrophobic Residues at the Intracellular Domain of the M2 Protein Play an Important Role in Budding and Membrane Integrity of Influenza Virus

Danqi Bao,^a Chenyang Lu,^{a,b} Tianxin Ma,^a Guanlong Xu,^c Yaqing Mao,^c Lingxiang Xin,^c Shiqi Niu,^a Zihua Wu,^a Xuesong Li,^a Qiaoyang Teng,^a  Zejun Li,^a  Qinfang Liu^a

^aShanghai Veterinary Research Institute, Chinese Academy of Agricultural Sciences, Shanghai, China

^bGuangxi Key Laboratory of Veterinary Biotechnology, Guangxi Veterinary Research Institute, Guangxi Province, People's Republic of China

^cChina Institute of Veterinary Drug Control, Beijing, People's Republic of China

Danqi Bao and Chenyang Lu contributed equally to this article. Author order was determined alphabetically by last name.

ABSTRACT M2 protein of influenza virus plays an important role in virus budding, including membrane scission and vRNP packaging. Three hydrophobic amino acids (91F, 92V, and 94I) at the intracellular domain of the M2 protein constitute a hydrophobic motif, also known as the LC3-interacting region (LIR), whereas the role of this motif remains largely unclear. To explore the role of the 91–94 hydrophobic motif for influenza virus, all three hydrophobic amino acids were mutated to either hydrophilic S or hydrophobic A, resulting in two mutant viruses (WSN-M2/SSS and WSN-M2/AAA) in the background of WSN/H1N1. The results showed that the budding ability of the M2/SSS protein was inhibited and the bilayer membrane integrity of the WSN-M2/SSS virion was impaired based on transmission electron microscopy (TEM), which in turn abolished the resistance to trypsin treatment. Moreover, the mutant WSN-M2/SSS was dramatically attenuated in mice. In contrast, the AAA mutations did not have a significant effect on the budding of the M2 proteins or the bilayer membrane integrity of the viruses, and the mutant WSN-M2/AAA was still lethal to mice. In addition, although the 91–94 motif is an LIR, knocking out of the LC3 protein of A549 cells did not significantly affect the membrane integrity of the influenza viruses propagated on the LC3KO cells, which suggested that the 91–94 hydrophobic motif affected the viral membrane integrity and budding is independent of the LC3 protein. Overall, the hydrophobicity of the 91–94 motif is crucial for the budding of M2, bilayer membrane integrity, and pathogenicity of the influenza viruses.

IMPORTANCE M2 plays a crucial role in the influenza virus life cycle. However, the function of the C-terminal intracellular domain of M2 protein remains largely unclear. In this study, we explored the function of the 91–94 hydrophobic motif of M2 protein. The results showed that the reduction of the hydrophobicity of the 91–94 motif significantly affected the budding ability of the M2 protein and impaired the bilayer membrane integrity of the mutant virus. The mouse study showed that the reduction of the hydrophobicity of the 91–94 motif significantly attenuated the mutant virus. All of the results indicated that the hydrophobicity of the 91–94 motif of the M2 protein plays an important role in budding, membrane integrity, and pathogenicity of influenza virus. Our study offers insights into the mechanism of influenza virus morphogenesis, particularly into the roles of the 91–94 hydrophobic motif of M2 in virion assembly and the pathogenicity of the influenza viruses.

KEYWORDS matrix protein 2, budding, hydrophobicity, membrane integrity, LC3-interacting region

Editor Stacey Schultz-Cherry, St. Jude Children's Research Hospital

Copyright © 2022 American Society for Microbiology. All Rights Reserved.

Address correspondence to Qinfang Liu, liuqinfang@shvri.ac.cn, or Zejun Li, lizejun@shvri.ac.cn.

The authors declare no conflict of interest.

Received 4 March 2022

Accepted 12 March 2022

Published 11 April 2022

Influenza virus poses a significant threat to public health and causes huge economic losses worldwide annually. Influenza virus, as a member of the *Orthomyxoviridae* family, has a segmented, negative-stranded RNA genome that encodes more than 10 viral proteins, including surface proteins (HA, NA, and M2), matrix protein 1 (M1), NS1, NS2, NP, and polymerase proteins (1). Influenza virus is an enveloped virus. All viral components are assembled at the cell membrane in an orderly manner and eventually are released from the infected cells through the budding process (2, 3).

Budding of the influenza virus is a result of coordination of the various viral components. Among all the viral components, only the surface membrane proteins (HA, NA, and M2) of influenza virus are capable of budding independently (4–6). At the beginning of the budding process, HA and NA proteins acting as initiators of the budding process are localized to the lipid raft on the cell membrane, and then cytoplasmic domains of the surface membrane proteins interact with M1 protein and recruit the vRNPs to the assembly site and eventually mediate progeny virion particle release from the cell membrane (7, 8).

M2 protein is a viral protein encoded by M gene of the influenza virus at the late stage of viral replication, and it contains 97 amino acid residues with an N-terminal extracellular domain, a transmembrane domain (TM), and a C-terminal intracellular domain containing an amphipathic helix (9, 10). The well-known function of M2 protein is ion channel activity that facilitates virion acidification for efficient uncoating during virus invasion (11, 12). M2 also is a cholesterol-binding protein and plays a critical role during viral budding process. The amphipathic helix (44–60) of M2 contains two overlapping cholesterol recognition amino acid consensus (CRAC) motifs (L/V-X1-5-Y-X1-5-R/K) (13, 14). The CRAC motif is responsible for cholesterol binding and membrane association. At the late stage of budding, the activity and orientation of the M2 amphipathic helix alters in a cholesterol-dependent manner, leading to an alteration of the membrane curvature at the neck of the budding virus, resulting in membrane scission and release of progeny virions (15).

The function of the C-terminal intracellular domain of M2 protein remains largely unknown. Previous studies reported that the 91 to 94 amino acids of the M2 intracellular domain formed a hydrophobic motif, named the LC3-interacting region (LIR) (16, 17). In the budding stage of influenza virus, M2 interacted with LC3 and relocated LC3 to the cell membrane via LIR motif and thereby blocked the formation of autophagic flux (18, 19). The M2 LIR is required for filamentous budding and virus stability, but the mechanism is unknown. The hydrophobic amino acids 91F, 92V, and 94I at the cytoplasmic domain of M2 protein are highly conserved in influenza A viruses (20, 21), whereas the role of the hydrophobic amino acids in replication and pathogenicity of influenza virus remains unclear.

In this study, our results showed that the loss of the hydrophobicity of the M2 protein 91–94 LIR motif impaired the integrity of bilayer membrane and significantly attenuated influenza virus. However, knocking out the LC3 protein (LC3-KO) did not affect the bilayer membrane integrity of influenza virus propagated on LC3-KO cells, which suggested that the viral bilayer membrane integrity and budding affected by the 91–94 hydrophobic motif is independent of the LC3 protein. Overall, the results indicated that the hydrophobicity of the M2 C terminus plays an important role in budding and pathogenicity of influenza viruses.

RESULTS

The 91–94 hydrophobic motif of M2 protein is critical for the pathogenicity of influenza virus. M2 protein contains a hydrophobic motif (91F, 92V, and 94I) at the C terminus, which is highly conserved in more than 99% of influenza A virus strains. To explore the function of the M2 91–94 hydrophobic motif of influenza viruses, the three hydrophobic amino acid residues 91F, 92V, and 94I of the hydrophobic motif of M2 were mutated to hydrophilic amino acid S or hydrophobic amino acid A (Fig. 1A). Two mutant viruses, WSN-M2/AAA and WSN-M2/SSS, were rescued in the background of WSN/H1N1, and the mutant viruses were verified by sequencing. To study the effects of M2 protein hydrophobic motif on replication of influenza viruses, virus growth curve

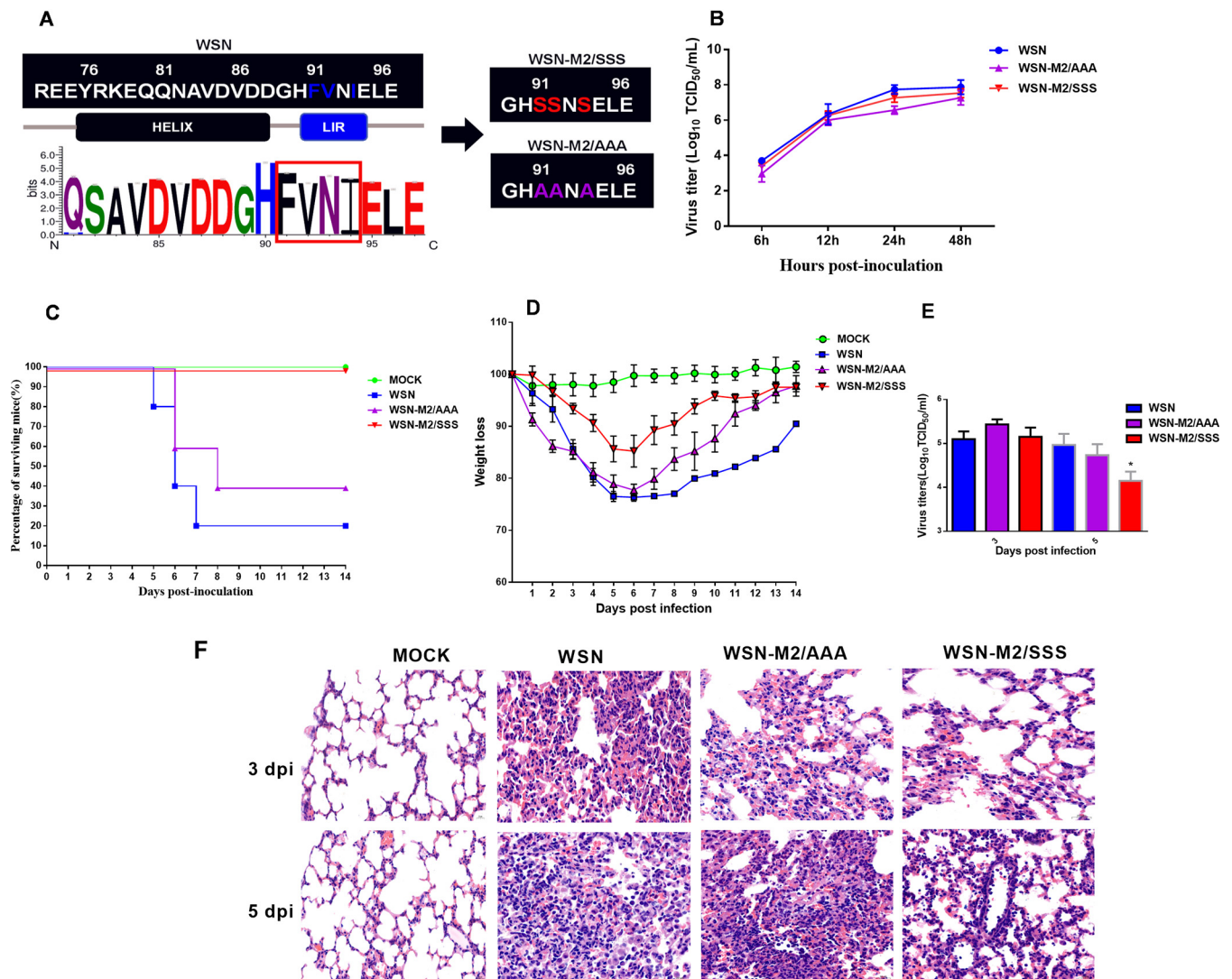


FIG 1 Effect of the M2 91–94 hydrophobic motif on the replication and pathogenicity of the influenza viruses. (A to F) Schematic diagram of the M2 protein 91–94 motif of the mutant viruses and conservation analysis of the M2 protein 91–94 motif of the influenza viruses (A); growth curves of the wild-type and mutant WSN viruses on MDCK cells (B); survival rate of mice infected with the wild type and mutant WSN viruses (C); weight loss of mice infected with the wild-type and mutant WSN viruses (D); replication of the wild-type and mutant WSN viruses in mouse lungs (E); histopathological study on mouse lungs harvested on 3 and 5 dpi; hematoxylin and eosin staining was performed (F).

was conducted on MDCK cells. The results showed that the replication levels of the mutant viruses WSN-M2/AAA and WSN-M2/SSS *in vitro* are similar to that of the wild-type WSN virus (Fig. 1B), which indicated that the mutation of the 91–94 hydrophobic motif does not have a significant impact on replication of influenza virus. To further explore the effects of the hydrophobic motif of M2 protein on pathogenicity of the influenza viruses, the virulence of the WSN and mutant viruses was evaluated in mice. The results showed that the wild-type WSN virus caused 80% mortality in infected mice within 7 days postinfection (dpi). The mortality rate of mice infected with the mutant virus WSN-M2/AAA was slightly reduced to 60%, whereas WSN-M2/SSS was no longer lethal to mice (Fig. 1C). The WSN-M2/SSS infection only caused slight weight loss in mice after infection compared with the other two infected groups (Fig. 1D). The virus loads in the mouse lungs showed that WSN-M2/AAA replicated to a level similar to that of the wild-type WSN virus, and the replication level of WSN-M2/SSS was much lower than those of the wild-type WSN and WSN-M2/AAA viruses at 5 dpi (Fig. 1E). In addition, the histopathologic examination showed that the infection with WSN-M2/SSS caused less inflammatory cell infiltration and alveolar structure damage in mouse lungs

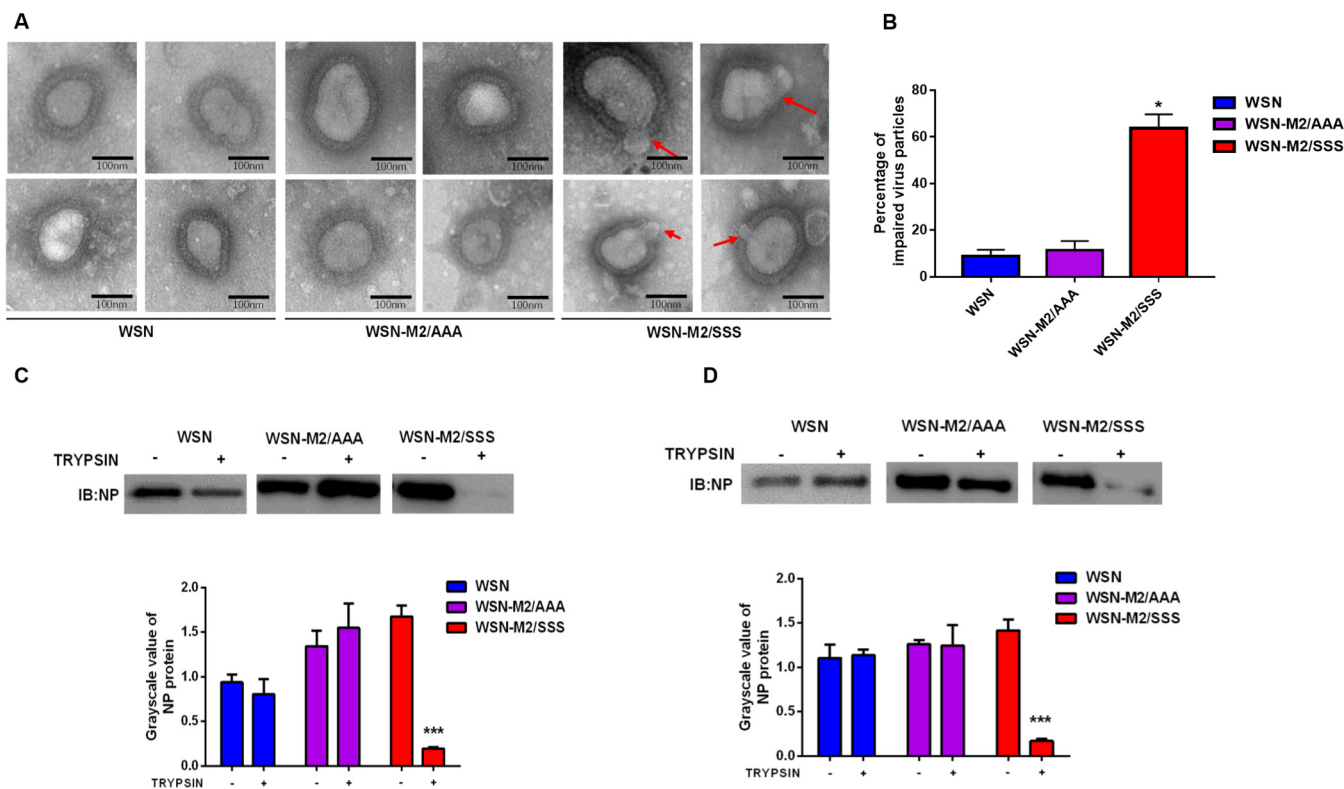


FIG 2 Effect of the M2 91–94 hydrophobic motif on trypsin resistance and bilayer membrane integrity of the influenza viruses. (A to D) Electron microscope observation of wild-type and mutant WSN viruses (A); percentage of virus particles of WSN, WSN-M2/AAA, and WSN-M2/SSS with impaired bilayer membrane under TEM (B); the NP detection of the wild-type and mutant WSN viruses propagated on MDCK cells after treated with trypsin (C); the NP detection of the wild-type and mutant WSN viruses propagated on SPF chicken embryos after treatment with trypsin (D). IB, immunoblot.

than wild-type WSN and WSN-M2/AAA (Fig. 1F). All of the results demonstrated that WSN-M2/SSS is significantly attenuated in mice compared with the wild-type WSN and WSN-M2/AAA viruses, which suggested that the hydrophobicity motif of M2 plays a critical role in the pathogenicity of influenza viruses.

The 91–94 hydrophobic motif of M2 affected the membrane integrity and trypsin resistance of the influenza viruses. To further study the role of the M2 91–94 hydrophobic motif in morphology of influenza virus, the purified virus particles propagated on MDCK cells were observed directly under a transmission electron microscope (TEM). The results showed that all three viruses are spherical. Interestingly, about 60% of the WSN-M2/SSS virus particles have humps on them without a clear bilayer lipid membrane, whereas neither the wild-type WSN nor WSN-M2/AAA virus particles had this phenomenon (Fig. 2A and B), which suggested that FVI-to-SSS mutations impair the integrity of the bilayer membrane of the mutant virions.

To further examine the viral membrane integrity of the three viruses, a trypsin resistance experiment was conducted. Purified wild-type and mutant viruses derived from MDCK cells and specific-pathogen-free (SPF) chicken embryos were treated with trypsin. NP protein was then detected by Western blotting after treatment. The results showed that the NP protein of the wild-type WSN and WSN-M2/AAA was significantly higher than that of WSN-M2/SSS after trypsin treatment. The NP protein was barely detected from the WSN M2/SSS that originated from MDCK or chicken embryos after trypsin treatment (Fig. 2C and D). The present results indicated that WSN-M2/SSS was more sensitive to trypsin than the wild-type WSN and WSN-M2/AAA, which confirmed that FVI/SSS mutations impaired the integrity of the bilayer membrane of the virion, resulting in loss of trypsin resistance of the mutant virus. All the results indicated that the reduced hydrophobicity of the M2 91–94 hydrophobic motif impaired the bilayer membrane integrity of the virus and decreased the virion trypsin resistance.

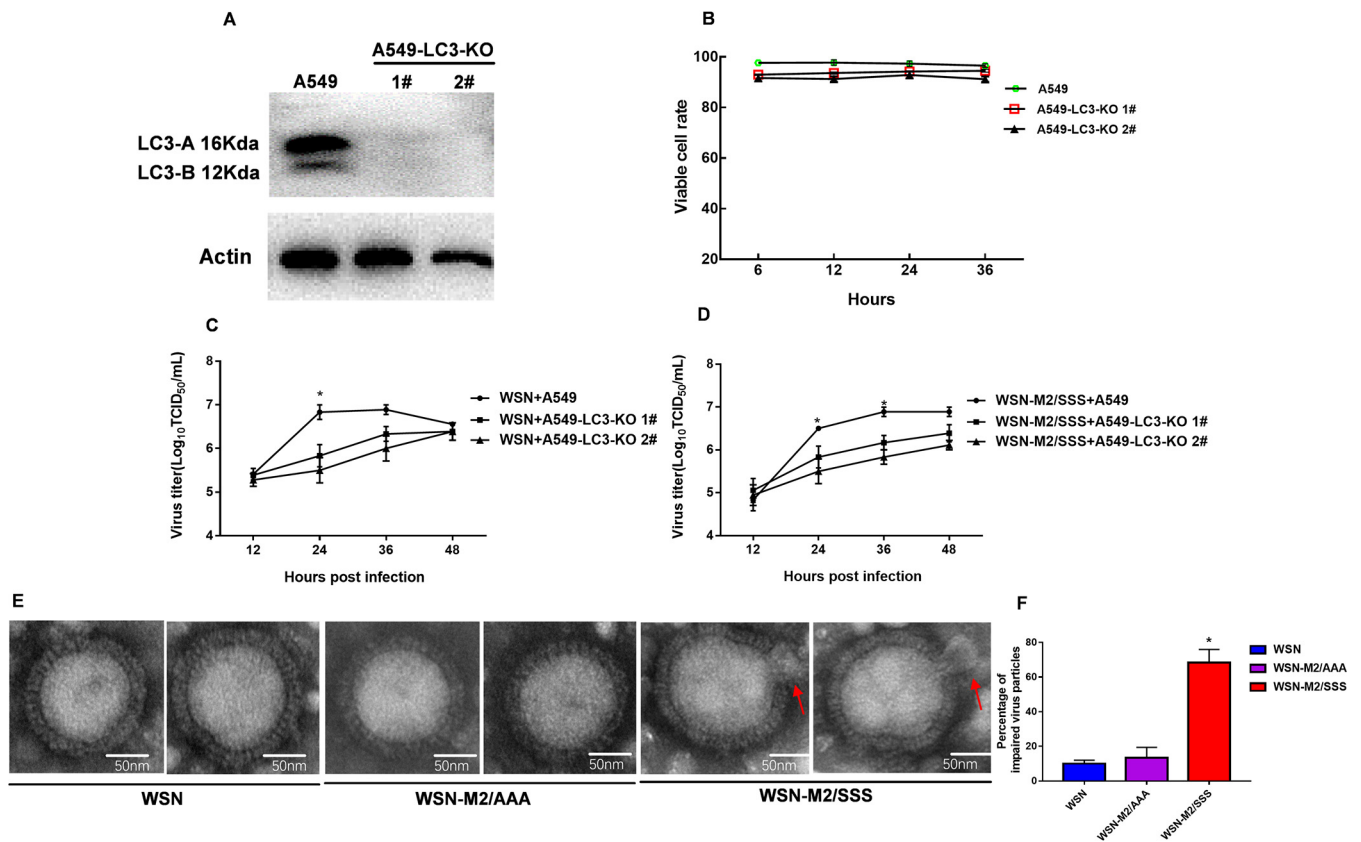


FIG 3 Effect of LC3 protein on the replication, trypsin resistance, and membrane integrity of the influenza viruses. (A to F) The LC3 protein detection of A549 and A549-LC3-KO cells (A); comparison of cell viability among A549 and two A549-LC3-KO cell clones (B); growth kinetics of WSN virus on A549 and two A549-LC3-KO cell clones (C); growth kinetics of the WSN-M2/SSS virus on A549 and two A549-LC3-KO cell clones (D); electron microscope observation of the WSN, WSN-M2/AAA, and WSN-M2/SSS viruses derived from A549 and A549-LC3-KO cells (E); percentage of the virus particles of WSN, WSN-M2/AAA, and WSN-M2/SSS with impaired bilayer membrane under TEM (F).

Host LC3 did not affect the membrane integrity of the influenza viruses. Previous studies showed that M2 blocked the formation of autophagic flux through interacting and relocating LC3 to the viral assembly site (14), whereas the influence of the host LC3 protein in replication and assembly of influenza virus remains unclear. In this study, two A549-LC3-KO cell clones were generated by CRISPR/Cas9 (Fig. 3A). The viability of the two A549-LC3-KO cell clones was not significantly different from that of the wild-type cells (Fig. 3B). Growth kinetics showed that the replication levels of the wild-type WSN and WSN-M2/SSS viruses in A549-LC3-KO were significantly lower than that in wild-type A549 at 24 h postinfection (hpi) (Fig. 3C and D), which suggested that LC3 facilitated the replication of the influenza viruses.

All three WSN, WSN-M2/AAA, and WSN-M2/SSS viruses propagated on A549-LC3-KO cells were purified and then subjected to transmission electron microscopy (TEM). The TEM results showed that both the WSN and WSN-M2/AAA viruses amplified on A549-LC3-KO cells are spherical and have intact bilayer membrane (Fig. 3E), while most of the WSN-M2/SSS virus particles (about 65%) have humps, which suggested that LC3 is not a determinant of the morphology and bilayer membrane integrity of the virions.

The 91–94 hydrophobic motif affected the budding capability of the M2 proteins. To further study the effect of the 91–94 hydrophobic motif on budding ability of the M2 proteins, Flag-M2, Flag-M2/AAA, and Flag-M2/SSS expression plasmids were transfected onto 293T cells. Cell lysates and virus-like particles (VLPs) in supernatant were collected for further analysis at 48 hpi. The results showed that the three M2 proteins have comparable expression levels in cells, whereas the level of Flag-M2/SSS is significantly lower than those of Flag-M2 and Flag-M2/AAA in the VLPs (Fig. 4A). The VLPs of the Flag-M2, Flag-M2/AAA, and Flag-M2/SSS purified from supernatant were evaluated

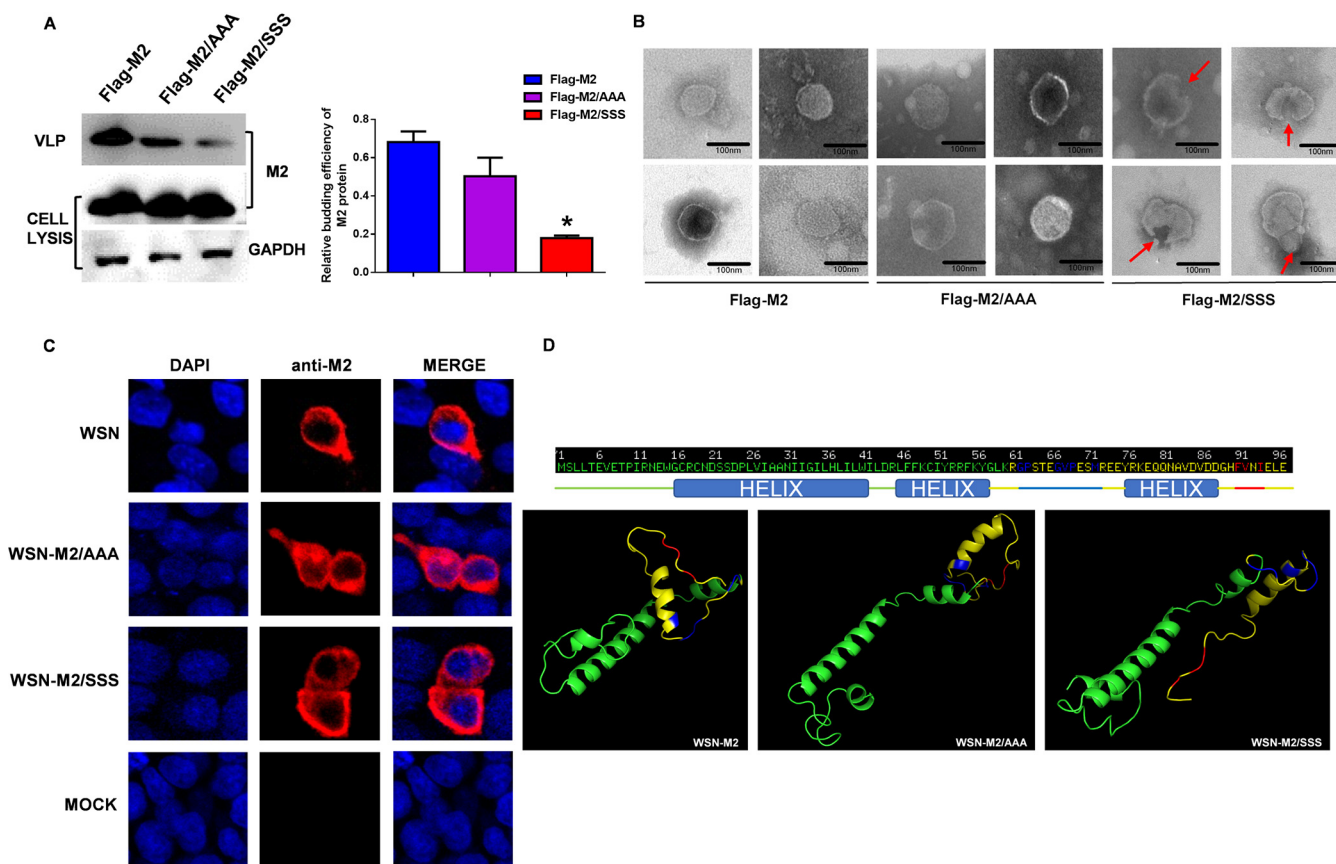


FIG 4 Effect of the 91–94 M2 hydrophobic motif on the budding capability and spatial structure of the M2 proteins. Protein detection in cell lysis and VLP samples of HEK293T cells transfected with Flag-M2, Flag-M2/AAA, and Flag-M2/SSS and relative budding efficiency of M2 protein in budding assay. (A to D) Relative budding efficiencies were determined by comparing the intensity of M2 protein bands in VLPs to those of protein bands in cell lysate by Western blotting (A); electron microscope observation of the VLPs of the Flag-M2, Flag-M2/AAA, and Flag-M2/SSS (B); subcellular localization of the M2, M2/AAA, and M2/SSS proteins in virus infected A549 cells by confocal microscopy (C); spatial structure prediction of the M2, M2/AAA, and M2/SSS (D). GAPDH, glyceraldehyde-3-phosphate dehydrogenase; DAPI, 4',6-diamidino-2-phenylindole.

under the electron microscope. The bilayer membranes of the Flag-M2 and Flag-M2/AAA VLP were intact. In contrast, the VLPs of Flag-M2/SSS were observed with damaged bilayer membrane (Fig. 4B). All these results indicated that the hydrophobicity motif is crucial for the budding ability of M2 and the membrane integrity of the VLPs.

To further explore whether the hydrophobicity loss of the 91–94 hydrophobic motif affects the cellular location of the M2 protein, WSN, WSN-M2/AAA, and WSN-M2/SSS were inoculated onto A549 cells. M2 proteins were observed by immunofluorescence assay (IFA). The results showed that the M2 proteins of all three viruses were localized on the cell membrane (Fig. 4C), which suggested that the hydrophobicity change did not hinder the membrane localization of M2.

To investigate whether the hydrophobicity motif is the key for the M2 C-terminal intracellular domain to maintain the spatial conformation. The spatial structures of WSN-M2, WSN-M2/SSS, and WSN-M2/AAA were modeled in the INTENSIVE mode of Phyre 2 as described previously (22). Different from the other three domains of M2 protein, the C-terminal intracellular domain is more flexible, with two motifs rich in hydrophobic amino acids: residues 60 to 70 and residues 91 to 94. The protein prediction results showed that the three predicted structures have about 70% accuracy. The 91–94 hydrophobic motif and the 60 to 70 residues of WSN-M2 and WSN-M2/AAA form a ring structure, which might be dependent on the hydrophobic interaction between these two peptides, whereas loss of hydrophobicity of 91–94 hydrophobic motif of M2 resulted in losing the ring structure, which might affect the function of M2 (Fig. 4D). All these results indicated that the 91–94 hydrophobic motif played an essential role in

maintenance of the spatial structure and budding capability of the M2 proteins and the membrane integrity of the influenza viruses.

DISCUSSION

M2 protein, as an important membrane protein, plays a crucial role in the replication cycle of influenza virus. M2 contains three domains: N-terminal extracellular domain, TM domain, and C-terminal intracellular domain (23). As a tetramer, the TM domain forms a four-helix proton channel that promotes uncoating of the virions (24). As for the C-terminal intracellular domain, the 44 to 60 residues compose an amphipathic helix that mediates the curvature of the cell membrane at the budding site and assists the viral particle budding (25), followed by the distal cytoplasmic tail, which is composed of 61 to 96 residues. However, the function and spatial structure of the M2 protein cytoplasmic tail remain largely unclear. In this study, the results indicated that the hydrophobicity of the 91–94 hydrophobic motif located in the C-terminal intracellular domain of the M2 protein played a critical role in the viral membrane integrity and pathogenicity of the influenza viruses.

M2 protein is located at the boundary between lipid raft and plasma membrane phase during viral budding (26). At the end of the budding process, it localizes at the neck of the budding virus particles (27) and produces a positive curvature of the plasma membrane, which can promote the membrane scission process to release the progeny virion (28). It has also been shown that the cytoplasmic tail at the C terminus plays a critical role in the membrane curvature regulation synergistically with the amphipathic helix (29). The amphipathic helix of M2 protein contains two partial overlapping cholesterol recognition amino acid consensus (CRAC) motifs (30). The M2 protein modifies membrane curvature in a cholesterol-dependent manner (31). Studies have shown that M2 produces positive membrane curvature in the presence of low levels of cholesterol environment, such as the bulk phase of the plasma membrane (32), whereas in an environment of high levels of cholesterol in the lipid raft-enriched sites of virus budding, M2 mediates negative membrane curvature (33). During initiation of the budding process, M2 was recruited to sites of virus budding and induced negative membrane curvature that stabilizes the positive membrane curvature caused by HA and M1 to facilitate the productive genome packaging and assembly of influenza virus (34). At the late stage of virus budding, M2 localized to the boundary between the lipid raft and the bulk plasma membrane phase, a lower-cholesterol environment that tends to cause positive membrane curvature to finish the membrane scission process (35, 36). In this study, the hydrophobicity loss of the 91–94 FVI impaired the budding ability of M2 and the membrane integrity of the influenza viruses and significantly attenuated the mutant viruses. Whether the hydrophobicity motif affects the cholesterol-binding and membrane scission activity of the amphipathic helix of M2 protein need further investigation.

Previous studies showed that the cytoplasmic tail of M2 interacts directly with the autophagy protein LC3 by a highly conserved LC3-interacting region (LIR 91–94) in M2. Mutations in LIR abolished LC3 binding, interfered with filamentous budding, and reduced virion stability (37–39). In this study, to explore the role of LC3 on replication and morphology of influenza virus, we generated an LC3 knockout A549 cell line. The WSN virus replicated to a lower titer on the A549-LC3-KO cell line than that on the wild-type A549 cells. However, knockout of the LC3 protein has no significant effect on the morphology and the bilayer membrane integrity of the virus particles. Together, our results evidenced that the LC3 protein was required for the efficient replication but not for the morphology and stability of the influenza viruses.

The C-terminal intracellular domain of M2 is a flexible structure (40), making its structure almost impossible to be directly observed by methods such as X-ray diffraction or nuclear magnetic resonance. The structural prediction showed that the intracellular region of M2 (60–96) forms a ring structure between two hydrophobic motifs (residues 60 to 70 and residues 91 to 94) with the helix in the middle, and the hydrophobicity of the 91–94 hydrophobic motif is important for M2 protein to maintain the intracellular domain structure. This ring structure might be necessary to the effective budding function of the M2 protein.

Taken together, in this study, we found that the reduction of the hydrophobicity in

the 91–94 hydrophobic motif at the M2 protein C terminus results in inhibited M2 protein budding ability and impaired bilayer membrane of the progeny virus particles, causing a decrease in virus pathogenicity. Therefore, the hydrophobicity of the 91–94 hydrophobic motif is necessary for the effective budding and the membrane integrity of the influenza viruses.

MATERIALS AND METHODS

Cells and viruses. Madin-Darby canine kidney (MDCK) cells were maintained in Eagle's minimal essential medium (EMEM) (Gibco, USA) with 5% fetal bovine serum (FBS) (Gibco, USA). Human embryonic kidney 293T cells and A549 cells were maintained in Dulbecco's modified Eagle medium (DMEM) (Gibco, USA) supplemented with 10% FBS. Influenza virus A/WSN/1933 H1N1 (WSN) was propagated and titrated on MDCK cells. To generate the mutant viruses, three hydrophobic amino acid residues, 91F, 92V, and 94I, of the hydrophobic motif of M2 were mutated to hydrophilic amino acid S or hydrophobic amino acid A (Fig. 1A). Two mutant viruses, WSN-M2/AAA and WSN-M2/SSS, were rescued in the background of WSN/H1N1, as described previously (41).

Generation of A549-LC3-KO cell line. Three pairs of single guide RNAs (sgRNAs) targeting LC3 protein genomic DNA sequence were designed and constructed on the LentiCRISPRv2 plasmid, and then we cotransfected HEK293T cells with the helper plasmids psPAX2 and VSVG. The supernatants were collected at 48 h posttransfection. The sequences of the sgRNAs are the following: LC3-sgRNA1, GTGATAATAGAACGATACAA; LC3-sgRNA2, TGAGCTCACTCATGTTGACA; LC3-sgRNA3, ATTCATCCCGAA CGTCTCC. A549 cells were infected with the lentivirus, and puromycin pressure (5 mg/mL) screening was performed on infected cells. After the puromycin pressure screening, the puromycin-resistant cells were subcloned to obtain the LC3 knockout A549 monoclonal cell line. The LC3 protein expression levels in two A549-LC3-KO cell clones and wild-type A549 cells were determined by Western blotting.

Growth kinetics. To compare virus replication, growth kinetics was determined as described previously (41). Briefly, MDCK, A549, or A549-LC3-KO cells were cultured overnight in 12-well plates and then infected with viruses at a multiplicity of infection (MOI) of 0.1. The cell supernatant was collected and titrated at different hpi for each time point in triplicates independently. The titers were determined on MDCK cells on a 96-well plate, and the 50% tissue culture infectious dose (TCID₅₀) was calculated with the Reed-Muench method.

VLP budding assay. VLP budding assay was conducted as described previously (41, 42). The M2 gene of WSN virus was constructed in pCDNA3.0 with an N-terminal Flag tag (Flag-M2). Mutations were introduced into amino acids 91, 92, and 94 of Flag-M2, resulting in Flag-M2/AAA (F91A/V92A/I94A) and Flag-M2/SSS (F91S/V92S/I94S) mutant plasmids. Five micrograms of Flag-M2, Flag-M2/AAA, or Flag-M2/SSS plasmid was transfected onto HEK293T cells cultured in 100-mm cell culture flasks. The supernatants were harvested at 48 h posttransfection and processed by centrifugation at $2,000 \times g$ for 20 min. The clarified supernatants were then layered on a 20% sucrose cushion and ultracentrifuged at $150,000 \times g$ for 4 h at 4°C in a Beckman ultracentrifuge (Fullerton, CA). The pellet was resuspended on ice in 50 μ L of phosphate-buffered saline (PBS). The M2 proteins in the cell lysate and in the VLP samples were detected by Western blotting with anti-Flag mouse monoclonal antibody.

Trypsin resistance assay. The wild-type and mutant WSN viruses were propagated on SPF chicken embryos and MDCK cells, respectively. The cell supernatant and chicken embryo allantoic fluid were collected at 48 hpi and processed by centrifugation at $2,000 \times g$ for 20 min. Clarified supernatants were then layered on a 20% sucrose cushion and ultracentrifuged at $150,000 \times g$ for 4 h at 4°C in a Beckman ultracentrifuge (Fullerton, CA). The pellet was resuspended on ice in 50 μ L of PBS and then treated with trypsin (Worthington) at a concentration of 100 μ g/mL and incubated at 37°C for 15 min, and then the NP protein was detected by Western blotting.

Western blotting. Protein samples were separated by loading to an SDS-polyacrylamide gel and transferred to an NC membrane. The membrane was blocked in PBS containing 5% bovine serum albumin for 30 min and then successively incubated with the indicated first antibody and horseradish peroxidase-conjugated secondary antibody (Thermo Fisher, USA). The immunoblot signals were visualized by using an enhanced chemiluminescence kit (Yeasen, China).

IFA. A549 cells cultured on chamber slides were infected with WSN, WSN-M2/AAA, and WSN-M2/SSS, respectively. All cells were fixed with 4% paraformaldehyde (PFA) and permeabilized with 0.1% Triton X-100 at 18 hpi. M2 protein was labeled with mouse anti-M2 antibody (Sigma, USA) followed by fluorescein isothiocyanate-conjugated anti-mouse IgG antibody (Invitrogen, USA). Confocal images were taken with a Leica TCS SP2 confocal microscope.

Animal study. To evaluate the effect of the hydrophobicity of the M2 protein 91–94 motif on pathogenicity of the viruses *in vivo*, the virulence of the wild-type and mutant WSN viruses were evaluated in a mouse model. Five-week-old female BALB/c mice were used with 11 mice in each group. The mice were infected intranasally with influenza virus (10^5 TCID₅₀/mouse). Three mice were euthanized and the lungs were collected at 3 and 5 days after infection. A portion of the lungs was used for histopathologic examination, and the virus titers in the rest of the lungs were titrated after homogenization. The body weight changes and deaths (a weight below 75% of the original weight is considered dead) of the remaining mice were recorded daily, and the mice were euthanized once the weight was lower than 75% of the initial body weight.

Transmission electron microscopy and structure modeling. All three wild-type and mutant WSN viruses were propagated on MDCK or A549-LC3-KO cells. To prepare the VLPs of the M2 and mutant proteins, the eukaryotic expression plasmids (Flag-M2, Flag-M2/AAA, and Flag-M2/SSS) were transfected to

HEK293T cells. The supernatants were collected at 48 h posttransfection. The propagated viruses and the cell supernatants were purified by density gradient centrifugation. Negative staining was prepared by pipetting the purified virus or VLP onto a grid, and after 30 s, we blotted the virus solution with Whatman paper. We added 1% phosphotungstic acid solution for 1 to 2 min. We blotted off the staining solution, added double-distilled H₂O to the grid, and then blotted it off. This was repeated three times, and then we allowed the grids to dry. These samples were examined in a Tecnai G2 Spirit BIOTWIN electron microscope, and the percentage of viruses with impaired bilayer membrane was determined based on observation of 100 virus particles under TEM, repeated three times for each virus. The three-dimensional structure of the wild-type and mutant M2 proteins was predicted in INTENSIVE mode by using the Phyre2 server as described previously (22) (<http://www.sbg.bio.ic.ac.uk/phyre2>).

Ethics statement and statistical analysis. All animals used in this study were taken care of in accordance with the guidelines of the Animal Care and Use Committee of Shanghai Veterinary Research Institute. All animal studies in this study were conducted in accordance with the guidelines of the Animal Care and Use Committee of Shanghai Veterinary Research Institute, and all animal study protocols are approved by the Chinese Academy of Agricultural Science (permit number SHVRI-Po-0120). All data were analyzed by using analysis of variance (ANOVA) in GraphPad Prism version 6.0 (GraphPad software Inc, CA). A *P* value of <0.05 was considered statistically significant.

ACKNOWLEDGMENTS

This study was supported by grants from the National Natural Science Foundation of China (no. 32172835, 32002273, 31772753, and 31572543), the Central Public-interest Scientific Institution Basal Research Fund (no. 2021JB03), and the Chinese Academy of Agricultural Sciences Young Talent Scientist Program (CAASQNYC-KYYJ-58).

REFERENCES

- Rossman JS, Lamb RA. 2011. Influenza virus assembly and budding. *Virology* 411:229–236. <https://doi.org/10.1016/j.virol.2010.12.003>.
- Nayak DP, Hui EK, Barman S. 2004. Assembly and budding of influenza virus. *Virus Res* 106:147–165. <https://doi.org/10.1016/j.virusres.2004.08.012>.
- Schmitt AP, Lamb RA. 2005. Influenza virus assembly and budding at the viral budzone. *Adv Virus Res* 64:383–416. [https://doi.org/10.1016/S0065-3527\(05\)64012-2](https://doi.org/10.1016/S0065-3527(05)64012-2).
- Chen BJ, Leser GP, Jackson D, Lamb RA. 2008. The influenza virus M2 protein cytoplasmic tail interacts with the M1 protein and influences virus assembly at the site of virus budding. *J Virol* 82:10059–10070. <https://doi.org/10.1128/JVI.01184-08>.
- Chen BJ, Leser GP, Morita E, Lamb RA. 2007. Influenza virus hemagglutinin and neuraminidase, but not the matrix protein, are required for assembly and budding of plasmid-derived virus-like particles. *J Virol* 81:7111–7123. <https://doi.org/10.1128/JVI.00361-07>.
- Leser GP, Lamb RA. 2005. Influenza virus assembly and budding in raft-derived microdomains: a quantitative analysis of the surface distribution of HA, NA and M2 proteins. *Virology* 342:215–227. <https://doi.org/10.1016/j.virol.2005.09.049>.
- Liu C, Eichelberger MC, Compans RW, Air GM. 1995. Influenza type A virus neuraminidase does not play a role in viral entry, replication, assembly, or budding. *J Virol* 69:1099–1106. <https://doi.org/10.1128/JVI.69.2.1099-1106.1995>.
- Nayak DP, Balogun RA, Yamada H, Zhou ZH, Barman S. 2009. Influenza virus morphogenesis and budding. *Virus Res* 143:147–161. <https://doi.org/10.1016/j.virusres.2009.05.010>.
- Manzoor R, Igarashi M, Takada A. 2017. Influenza A virus M2 Protein: roles from ingress to egress. *Int J Mol Sci* 18:e122649. <https://doi.org/10.3390/ijms18122649>.
- Wohlgemuth N, Lane AP, Pekosz A. 2018. Influenza A virus M2 protein apical targeting is required for efficient virus replication. *J Virol* 92:e01425-18. <https://doi.org/10.1128/JVI.01425-18>.
- Duncan MC, Onguene PA, Kihara I, Nebangwa DN, Naidu ME, Williams DE, Balgi AD, Andrae-Marobela K, Roberge M, Andersen RJ, Niikura M, Ntie-Kang F, Tietjen I. 2020. Virtual screening identifies chebulagic acid as an inhibitor of the M2(S31N) viral ion channel and influenza A virus. *Molecules* 25:e122903. <https://doi.org/10.3390/molecules25122903>.
- Vorobjev YN. 2020. Design of an efficient inhibitor for the influenza A virus M2 ion channel. *Mol Biol (Mosk)* 54:321–332. <https://doi.org/10.31857/S0026898420020160>.
- Martyna A, Bahsoun B, Madsen JJ, Jackson F, Badham MD, Voth GA, Rossman JS. 2020. Cholesterol alters the orientation and activity of the influenza virus M2 amphipathic helix in the membrane. *J Phys Chem B* 124:6738–6747. <https://doi.org/10.1021/acs.jpcc.0c03331>.
- Roberts KL, Leser GP, Ma C, Lamb RA. 2013. The amphipathic helix of influenza A virus M2 protein is required for filamentous bud formation and scission of filamentous and spherical particles. *J Virol* 87:9973–9982. <https://doi.org/10.1128/JVI.01363-13>.
- Elkins MR, Williams JK, Gelenter MD, Dai P, Kwon B, Sergeev IV, Pentelute BL, Hong M. 2017. Cholesterol-binding site of the influenza M2 protein in lipid bilayers from solid-state NMR. *Proc Natl Acad Sci U S A* 114:12946–12951. <https://doi.org/10.1073/pnas.1715127114>.
- Beale R, Wise H, Stuart A, Ravenhill BJ, Digard P, Randow F. 2014. A LC3-interacting motif in the influenza A virus M2 protein is required to subvert autophagy and maintain virion stability. *Cell Host Microbe* 15:239–247. <https://doi.org/10.1016/j.chom.2014.01.006>.
- Gannage M, Dormann D, Albrecht R, Denjtel J, Torossi T, Ramer PC, Lee M, Strowig T, Arrey F, Conenello G, Pypaert M, Andersen J, Garcia-Sastre A, Munz C. 2009. Matrix protein 2 of influenza A virus blocks autophagosome fusion with lysosomes. *Cell Host Microbe* 6:367–380. <https://doi.org/10.1016/j.chom.2009.09.005>.
- Rossman JS, Lamb RA. 2009. Autophagy, apoptosis, and the influenza virus M2 protein. *Cell Host Microbe* 6:299–300. <https://doi.org/10.1016/j.chom.2009.09.009>.
- Zhang R, Chi X, Wang S, Qi B, Yu X, Chen JL. 2014. The regulation of autophagy by influenza A virus. *Biomed Res Int* 2014:498083. <https://doi.org/10.1155/2014/498083>.
- Zhirnov OP, Klenk HD. 2013. Influenza A virus proteins NS1 and hemagglutinin along with M2 are involved in stimulation of autophagy in infected cells. *J Virol* 87:13107–13114. <https://doi.org/10.1128/JVI.02148-13>.
- Wang R, Zhu Y, Zhao J, Ren C, Li P, Chen H, Jin M, Zhou H. 2019. Autophagy promotes replication of influenza A virus in vitro. *J Virol* 93:e01984-18. <https://doi.org/10.1128/JVI.01984-18>.
- Kelley LA, Mezulis S, Yates CM, Wass MN, Sternberg MJ. 2015. The Phyre2 web portal for protein modeling, prediction and analysis. *Nat Protoc* 10:845–858. <https://doi.org/10.1038/nprot.2015.053>.
- Torabifard H, Panahi A, Brooks CL, III. 2020. M2 amphipathic helices facilitate pH-dependent conformational transition in influenza A virus. *Proc Natl Acad Sci U S A* 117:3583–3591. <https://doi.org/10.1073/pnas.1913385117>.
- Manzoor R, Eguchi N, Yoshida R, Ozaki H, Kondoh T, Okuya K, Miyamoto H, Takada A. 2020. A novel mechanism underlying antiviral activity of an influenza virus M2-specific antibody. *J Virol* 95:e01277-20. <https://doi.org/10.1128/JVI.01277-20>.
- Ciampor F, Cmarko D, Cmarkova J, Zavodska E. 1995. Influenza virus M2 protein and haemagglutinin conformation changes during intracellular transport. *Acta Virol* 39:171–181.

26. Hu B, Siche S, Moller L, Veit M. 2020. Amphipathic helices of cellular proteins can replace the helix in M2 of influenza A virus with only small effects on virus replication. *J Virol* 94:e01605-19. <https://doi.org/10.1128/JVI.01605-19>.
27. Wang JF, Chou KC. 2012. Recent advances in computational studies on influenza A virus M2 proton channel. *Mini Rev Med Chem* 12:971–978. <https://doi.org/10.2174/138955712802762275>.
28. Rossman JS, Jing X, Leser GP, Lamb RA. 2010. Influenza virus M2 protein mediates ESCRT-independent membrane scission. *Cell* 142:902–913. <https://doi.org/10.1016/j.cell.2010.08.029>.
29. Leser GP, Lamb RA. 2017. Lateral organization of influenza virus proteins in the budzone region of the plasma membrane. *J Virol* 91:e02104-16. <https://doi.org/10.1128/JVI.02104-16>.
30. Schroeder C, Heider H, Moncke-Buchner E, Lin TI. 2005. The influenza virus ion channel and maturation cofactor M2 is a cholesterol-binding protein. *Eur Biophys J* 34:52–66. <https://doi.org/10.1007/s00249-004-0424-1>.
31. Thaa B, Tiesch C, Moller L, Schmitt AO, Wolff T, Bannert N, Herrmann A, Veit M. 2012. Growth of influenza A virus is not impeded by simultaneous removal of the cholesterol-binding and acylation sites in the M2 protein. *J Gen Virol* 93:282–292. <https://doi.org/10.1099/vir.0.038554-0>.
32. Thaa B, Siche S, Herrmann A, Veit M. 2014. Acylation and cholesterol binding are not required for targeting of influenza A virus M2 protein to the hemagglutinin-defined budzone. *FEBS Lett* 588:1031–1036. <https://doi.org/10.1016/j.febslet.2014.02.014>.
33. Kim SS, Upshur MA, Saotome K, Sahu ID, McCarrick RM, Feix JB, Lorigan GA, Howard KP. 2015. Cholesterol-dependent conformational exchange of the C-terminal domain of the influenza A M2 protein. *Biochemistry* 54:7157–7167. <https://doi.org/10.1021/acs.biochem.5b01065>.
34. Veglia G, Nelson SE, Gopinath T. 2016. Allosteric regulation of the M2 protein from influenza A by cholesterol. *Biophys J* 110:1207–1208. <https://doi.org/10.1016/j.bpj.2016.01.034>.
35. Thaa B, Levental I, Herrmann A, Veit M. 2011. Intrinsic membrane association of the cytoplasmic tail of influenza virus M2 protein and lateral membrane sorting regulated by cholesterol binding and palmitoylation. *Biochem J* 437:389–397. <https://doi.org/10.1042/BJ20110706>.
36. Stewart SM, Wu WH, Lalime EN, Pekosz A. 2010. The cholesterol recognition/interaction amino acid consensus motif of the influenza A virus M2 protein is not required for virus replication but contributes to virulence. *Virology* 405:530–538. <https://doi.org/10.1016/j.virol.2010.06.035>.
37. Mehrbod P, Ande SR, Alizadeh J, Rahimizadeh S, Shariati A, Malek H, Hashemi M, Glover KKM, Sher AA, Coombs KM, Ghavami S. 2019. The roles of apoptosis, autophagy and unfolded protein response in arbovirus, influenza virus, and HIV infections. *Virulence* 10:376–413. <https://doi.org/10.1080/21505594.2019.1605803>.
38. Yamauchi Y. 2020. Influenza A virus uncoating. *Adv Virus Res* 106:1–38. <https://doi.org/10.1016/bs.aivir.2020.01.001>.
39. Yeganeh B, Ghavami S, Rahim MN, Klonisch T, Halayko AJ, Coombs KM. 2018. Autophagy activation is required for influenza A virus-induced apoptosis and replication. *Biochim Biophys Acta Mol Cell Res* 1865:364–378. <https://doi.org/10.1016/j.bbamcr.2017.10.014>.
40. Kim G, Raymond HE, Herneisen AL, Wong-Rolle A, Howard KP. 2019. The distal cytoplasmic tail of the influenza A M2 protein dynamically extends from the membrane. *Biochim Biophys Acta Biomembr* 1861:1421–1427. <https://doi.org/10.1016/j.bbamem.2019.05.021>.
41. Bao D, Xue R, Zhang M, Lu C, Ma T, Ren C, Zhang T, Yang J, Teng Q, Li X, Li Z, Liu Q. 2021. N-linked glycosylation plays an important role in budding of neuraminidase protein and virulence of influenza viruses. *J Virol* 95:e02042-20. <https://doi.org/10.1128/JVI.02042-20>.
42. Wang D, Harmon A, Jin J, Francis DH, Christopher-Hennings J, Nelson E, Montelaro RC, Li F. 2010. The lack of an inherent membrane targeting signal is responsible for the failure of the matrix (M1) protein of influenza A virus to bud into virus-like particles. *J Virol* 84:4673–4681. <https://doi.org/10.1128/JVI.02306-09>.